AIAA 2002–0591

Detached-Eddy Simulation of Fighter Aircraft at High Alpha

James R. Forsythe
United States Air Force Academy, Department of Aeronautics, Colorado Spring, CO 80840

Kyle D. Squires
MAE Department, Arizona State University, Tempe, AZ 85287

Kenneth E. Wurtzler
Cobalt Solution, LLC, Miamisburg, OH 45459

Philippe R. Spalart
Boeing Commercial Airplanes, Seattle, WA 98124

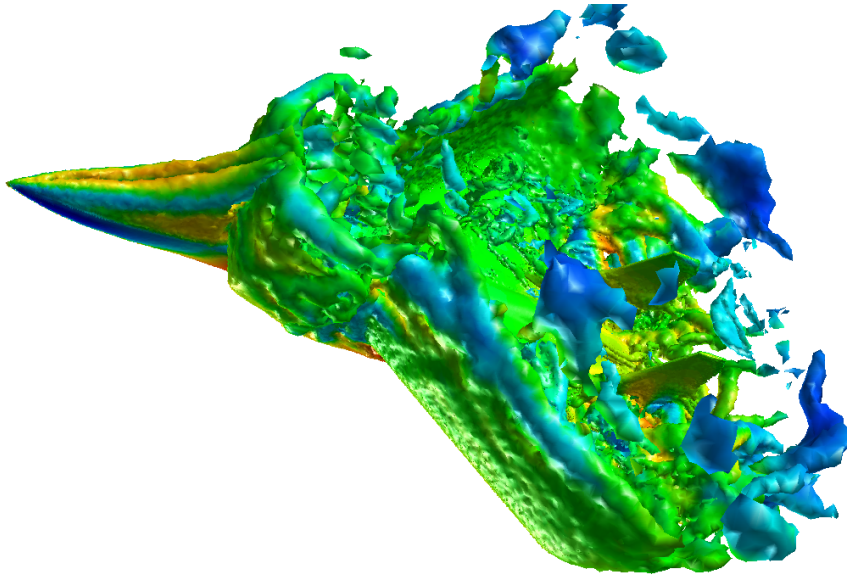

Aerospace Sciences Meeting 2002
14–18 January 2002 / Reno, Nevada

Detached-Eddy Simulation of Fighter Aircraft at High Alpha

James R. Forsythe*
United States Air Force Academy, Department of Aeronautics, Colorado Spring, CO 80840
Kyle D. Squires†
MAE Department, Arizona State University, Tempe, AZ 85287
Kenneth E. Wurtzler ‡
Cobalt Solution, LLC, Miamisburg, OH 45459
Philippe R. Spalart§
Boeing Commercial Airplanes, Seattle, WA 98124

Detached-Eddy Simulation (DES) is used to predict the massively separated flow around an F-15E at 65° angle-of-attack. The calculations are performed at flight test conditions corresponding to a chord-based Reynolds number of 13.6×10^6 and Mach number of 0.3. Flow field solutions are obtained using using Cobalt. The calculations were performed using unstructured grids in which the baseline mesh is comprised of 5.9×10^6 cells with prisms in the boundary layers and isotropic tetrahedra in other regions. Mesh spacings from solid surfaces to the first cell center nearest the wall were within one viscous unit. Baseline calculations were performed on a half aircraft by assuming symmetry. Modeling the full aircraft by mirroring the grid across the symmetry plane was compared to the baseline calculations. The influence of the mesh size was assessed using calculations performed on two other grids: a coarser grid of 2.85×10^6 cells and a finer mesh of 10×10^6 cells. In addition, the influence of the timestep is investigated using the baseline mesh and two simulations with timesteps a factor of two and a factor of four larger than the the value used in the baseline calculations.

DES predictions are assessed via comparison to Boeing's stability and control database as well as solutions on the same grids of the Reynolds-averaged Navier-Stokes (RANS) equations.

Both RANS and DES predictions have only a weak dependence for integrated forces on the grid density for the range examined, suggesting a grid-converged solution. DES predictions show that the wake region is characterized by complex and chaotic three-dimensional structures exhibiting a reasonable range of length and time scales. Time-dependent RANS predictions were obtained using the Spalart-Allmaras model and evolve to steady solutions. In general, both RANS and DES predictions of averaged quantities exhibit favorable agreement with the flight-test data. DES predictions of the lift, drag, and pitching moment coefficients, which were averaged over as many as 150 inertial timescales, agree more favorably with the flight-test data than the RANS results, although both methods are within 10% of the stability and control database.

Introduction

NUMERICAL simulation of the flow around complex configurations offers a powerful tool for analysis, e.g., a means to screen configurations prior to costly and time-consuming flight tests. One example is in spin testing in which Computational Fluid Dynamics (CFD) could be used to provide detailed information on stability, spin modes, etc. Such information could be difficult or impossible to extract from flight tests and a numerical tool would be clearly useful. While the over-arching goal of the current effort is development of a CFD tool for spin analysis, aircraft spin strongly challenges numerical models. The flow fields encountered are three-dimensional, massively separated, and unsteady. In addition, because Reynolds number effects are important for spin testing, calculations should be performed at flight test conditions.

The current effort focuses on the F-15E because of the availability of an extensive stability and control database.[1] This database was compiled from an extensive series of flight tests, including spins. Gaps in the flight test were filled in with wind tunnel testing. In this contribution, it is the static aircraft at 65° angle of attack that is the primary focus of the calculations. This angle-of-attack is chosen since it is the angle that a clean F-15E will maintain a stable spin.

Most current engineering approaches to predic-

*Assistant Professor, Member AIAA
†Professor, Member of AIAA
‡Vice President, Member of AIAA
§Senior Scientist

tion of unsteady flows are based on solution of the Reynolds-averaged Navier-Stokes (RANS) equations. The turbulence models employed in RANS methods necessarily parameterize the entire spectrum of turbulent motions. While often adequate in steady flows with no regions of flow reversal, or possibly exhibiting shallow separations, it appears inevitable that RANS turbulence models are unable to accurately predict phenomena dominating flows characterized by massive separations. Unsteady massively separated flows are characterized by geometry-dependent and three-dimensional turbulent eddies. These eddies, arguably, are what defeats RANS turbulence models, of any complexity.

To overcome the deficiencies of RANS models for predicting massively separated flows, Spalart *et al.*[2] proposed Detached-Eddy Simulation (DES) with the objective of developing a numerically feasible and accurate approach combining the most favorable elements of RANS models and Large Eddy Simulation (LES). The primary advantage of DES is that it can be applied at high Reynolds numbers as can Reynolds-averaged techniques, but also resolves geometry-dependent, unsteady three-dimensional turbulent motions as in LES. DES predictions to date have been favorable, forming one of the motivations for this research. The specific aims are to apply and assess DES, consistent with the long-term goal of developing a CFD tool for analysis and prediction of aircraft spin. The application under consideration is prediction of the time-dependent flow around a complete aircraft - the F-15E at 65° angle of attack. The goal is to assess DES predictions against both measurements and predictions of the same configuration obtained using a RANS turbulence model.

For calculations of complex configurations and at high Reynolds numbers, high performance computation is essential. In this work, solutions of the compressible Navier-Stokes equations on unstructured grids are obtained using Cobalt.[3] The numerical method is based on a finite-volume approach and is second-order accurate in space and time. The method is point-implicit and permits CFL numbers as large as one million for steady-state computations.[5] Turbulence-resolving simulations are necessarily time dependent and for DES predictions the code is run in a time-accurate fashion. The computations are performed in parallel using the Message Passing Interface.[4] For feature-resolving techniques such as DES, important in assessment of the predictions is sensitivity to both mesh refinement as well as the computational timestep. Presented in subsequent sections is a reasonably comprehensive grid and timestep refinement study.

Computational Approach

Spalart-Allmaras Model

The Spalart-Allmaras (referred to as 'S-A' throughout) one-equation model[6] solves a single partial differential equation for a variable $\widetilde{\nu}$ which is related to the turbulent viscosity. The differential equation is derived by "using empiricism and arguments of dimensional analysis, Galilean invariance and selected dependence on the molecular viscosity."[6] The model includes a wall destruction term that reduces the turbulent viscosity in the log layer and laminar sublayer and trip terms that provides a smooth transition from laminar to turbulent flow. In the present computations, the trip term was not active,

$$\begin{aligned}\frac{D\widetilde{\nu}}{Dt} &= c_{b1}\widetilde{S}\,\widetilde{\nu} - c_{w1} f_w \left[\frac{\widetilde{\nu}}{d}\right]^2 \\ &\quad + \frac{1}{\sigma}\left[\nabla\cdot\left(\left(\nu+\widetilde{\nu}\right)\nabla\widetilde{\nu}\right) + c_{b2}\left(\nabla\widetilde{\nu}\right)^2\right]\end{aligned} \tag{1}$$

The turbulent viscosity is determined via,

$$\nu_t = \widetilde{\nu}\; f_{v1}, \qquad f_{v1} = \frac{\chi^3}{\chi^3 + c_{v1}^3}, \qquad \chi \equiv \frac{\widetilde{\nu}}{\nu}, \tag{2}$$

where ν is the molecular viscosity. Using S to denote the magnitude of the vorticity, the modified vorticity $\widetilde{S}$ is defined as,

$$\widetilde{S} \equiv S + \frac{\widetilde{\nu}}{\kappa^2 d^2} f_{v2}\,, \qquad f_{v2} = 1 - \frac{\chi}{1+\chi f_{v1}}\,, \tag{3}$$

where d is the distance to the closest wall. The wall destruction function, f_w is,

$$f_w = g\left[\frac{1+c_{w3}^6}{g^6 + c_{w3}^6}\right]^{\frac{1}{6}} \tag{4}$$

$$g = r + c_{w2}(r^6 - r)\,, \qquad r \equiv \frac{\widetilde{\nu}}{\widetilde{S}\kappa^2 d^2}\,. \tag{5}$$

The closure coefficients are given by:

$$\begin{array}{ccc} c_{b1} = 0.1355 & \sigma = \frac{2}{3} & c_{b2} = 0.622 \\ \kappa = 0.41 & c_{w1} = \frac{c_{b1}}{\kappa^2} + \frac{(1+c_{b2})}{\sigma} & c_{w2} = 0.3 \\ c_{w3} = 2 & c_{v1} = 7.1 & \end{array} \tag{6}$$

Detached-Eddy Simulation

The three-dimensional and time-dependent flow around the F-15E is predicted using Detached-Eddy Simulation. The DES formulation in this study is based on a modification to the Spalart-Allmaras RANS model[6] such that the model reduces to its RANS formulation near solid surfaces and to a subgrid model away from the wall.[7] The basis is to attempt to take advantage of the usually adequate performance of RANS models in the thin shear layers where these models are calibrated and the power of LES for resolution of geometry-dependent and three-dimensional

eddies. The DES formulation is obtained by replacing in the S-A model the distance to the nearest wall, d, by $\widetilde{d}$, where $\widetilde{d}$ is defined as,

$$\widetilde{d} \equiv \min(d, C_{DES}\Delta)\,. \tag{7}$$

In Eqn. (7) for the current study, Δ is the largest distance between the cell center under consideration and the cell center of the neighbors (i.e., those cells sharing a face with the cell in question). In "natural" applications of DES, the wall-parallel grid spacings (e.g., streamwise and spanwise) are at least on the order of the boundary layer thickness and the S-A RANS model is retained throughout the boundary layer, i.e., $\widetilde{d} = d$. Consequently, prediction of boundary layer separation is determined in the 'RANS mode' of DES. Away from solid boundaries, the closure is a one-equation model for the SGS eddy viscosity. When the production and destruction terms of the model are balanced, the length scale $\widetilde{d} = C_{DES}\Delta$ in the LES region yields a Smagorinsky eddy viscosity $\widetilde{\nu} \propto S\Delta^2$. Analogous to classical LES, the role of Δ is to allow the energy cascade down to the grid size; roughly, it makes the pseudo-Kolmogorov length scale, based on the eddy viscosity, proportional to the grid spacing. The additional model constant $C_{DES} = 0.65$ was set in homogeneous turbulence[8] and is used without modification in this study.

Numerical Approach

Code Details

The computations were performed using using Cobalt$_{60}$[3] and Cobalt. Cobalt is a commercial version of Cobalt$_{60}$ (a Navier-Stokes solver developed at the Air Force Research Laboratory). The improvements to the commercial version relevant to this study were the ability to compute time-averages and turbulent statistics, faster per-iteration times, an improved spatial operator, and improved temporal integration. Additionally, Cobalt is capable of computing geometries undergoing rigid body motion, a crucial feature required to spin the aircraft in subsequent simulations. The timestep study was performed using Cobalt$_{60}$, while the grid refinement study was performed using Cobalt.

Cobalt is an unstructured finite-volume method developed for solution of the compressible Navier-Stokes equations and described in Strang *et al.*[3] The numerical method is a cell-centered finite volume approach applicable to arbitrary cell topologies (e.g, hexahedrals, prisms, tetrahdrons). The spatial operator uses the exact Reimann Solver of Gottlieb and Groth,[9] least squares gradient calculations using QR factorization to provide second order accuracy in space, and TVD flux limiters to limit extremes at cell faces. A point implicit method using analytic first-order inviscid and viscous Jacobians is used for advancement of the discretized system. For time-accurate computations, a Newton sub-iteration scheme is employed, the method is second order accurate in time.

For parallel performance, Cobalt uses the domain decomposition library ParMETIS[10] to provide nearly perfect load balancing with a minimal surface interface between zones. Communication between processors is achieved using Message Passing Interface (MPI), with parallel efficiencies above 95% on as many as 1024 processors.[4]

In the calculations presented in this manuscript, a minimum of two Newton sub-iterations were used for all time accurate calculations, which roughly doubles the cost of each step compared to a steady-state computation, but is necessary to ensure time accuracy (steady state calculations are performed with zero or one sub-iteration). In addition, to obtain sufficient samples in the averages, statistics were acquired over a minimum of 100 time units (L/V_∞). With the (dimensionless) timestep usually set to 0.01. Steady state calculations require on average about 2,000 iterations for convergence.

Experience with the method and code has been developed through previous DES applications to predictions of the flow over a rounded-corner square,[11] supersonic axisymmetric base,[12] and section of a NACA 0012 airfoil. Super-critical solutions of the flow over the rounded-corner square agreed well with experimental pressure measurements in contrast to large errors in RANS and LES calculations.[11] DES predictions of the supersonic axisymmetric base flow[12] showed good agreement to experimental base pressures and off body turbulent kinetic energy. A code-to-code comparison was accomplished through prediction of a NACA 0012 airfoil section. Cobalt calculations were performed using the same grid and with the same timestep as in Shur *et al.*[8] Unsteady lift and drag coefficient histories are shown in Figure 1 for calculations at a chord-based Reynolds number of 10^5. In both figures the time axis is made dimensionless using the chord length and velocity of the freestream. As shown in the figure, an interesting feature of the lift and drag histories in Shur *et al.*[8] is the relatively strong modulation of the forces, an effect also produced in the Cobalt solutions. In addition, the mean values for both C_l and C_d agree well between the two calculations.

Grid Generation

A baseline grid for half of the F-15E was created using VGRIDns[13] and is shown in Figures 2 and 3. The original grid consisted of 7.9×10^6 tetrahedral cells. Using the grid utility *blacksmith* developed by the Air Force Research Laboratories Air Vehicles Directorate, nine layers in the boundary layer were combined into prisms, reducing the total number of cells to 5.9×10^6 for the baseline mesh. The distance from solid surfaces to the first cell center normal to the wall was constant, resulting in an average distance in wall units of 0.7.

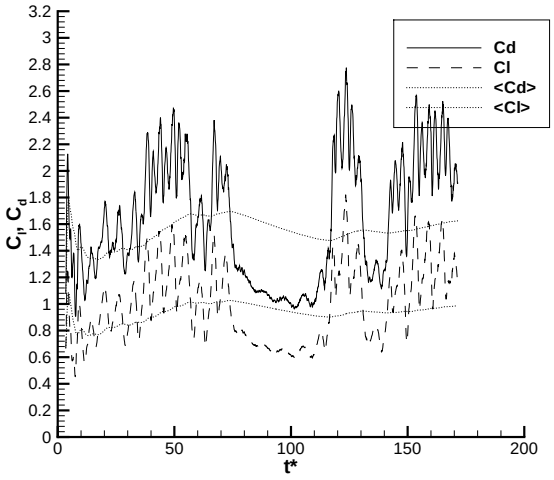

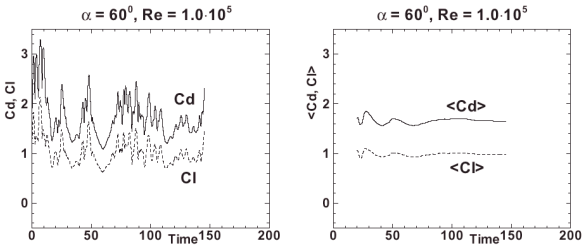

Fig. 1 DES predictions of lift and drag coefficients over the NACA 0012 airfoil section at 60° angle-of-attack, $Re = 10^5$. Cobalt solutions in the top frame show the instantaneous lift and drag along with the running time average. Predictions from Shur *et al.*[8] in the bottom frames show the instantaneous lift and drag on the left and running average on the right.

Cell growth in the wall-normal direction was specified using a geometric stretching factor of 1.3. There were approximately 160,000 faces on the surface of the aircraft with only a few hundred cells on the outer boundary, as seen in Figure 2. Currently, the engine inlet and exhaust are set to a no-slip boundary condition. At an early phase of the study, modeling the inlet with a mass flow boundary condition was attempted. For the flow at 65° angle-of-attack, a separation bubble formed, which impinged on the inlet boundary. This in turn lead to numerical problems since the flow was both entering and exiting a boundary at which a mass flow boundary condition was being applied. An important aspect of future work will be extension of the inlet geometry and to model the flow through the engine.

An advantage of an unstructured grid in DES is that

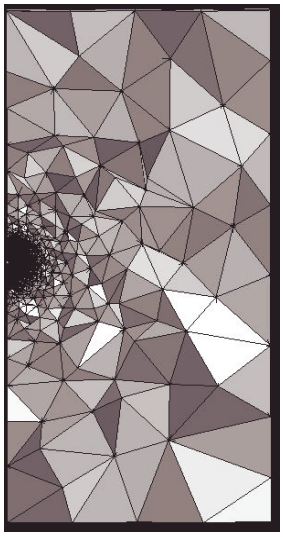

Fig. 2 Far-field view of the baseline mesh.

the tetrahedra outside the boundary layer are nearly isotropic, such cell-types sometimes difficult to achieve using a structured approach. Isotropic cells ensure the lowest value of Δ for a given cell volume, lowering the eddy viscosity and allowing more fluctuations to be resolved on the mesh. Also, since the orientation of turbulent structures are not necessarily known *a priori*, isotropic cells are a logical approach to representing the turbulence.

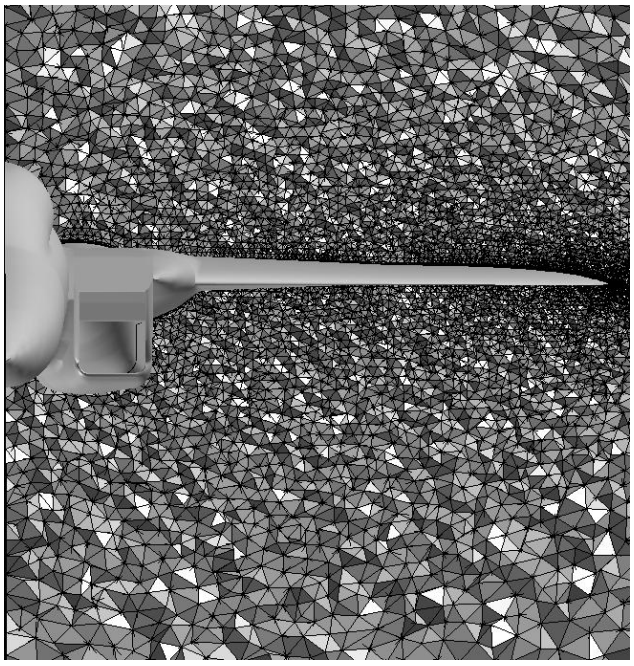

Fig. 3 Baseline computational mesh near aircraft surface.

Sensitivity to the mesh was examined via computations using two additional grids (see Figures 4 through 6), one coarser and the other finer than the baseline mesh. Generation of the baseline grid re-

quired one week using VGRIDns.[13] Each additional grid was created in one day. VGRIDns uses "background sources" to define grid spacing. The cell spacing at any location in the grid is a function of the distance to each source, the source strengths, and the source spacing. VGRIDns allows the spacing for all the sources to be multiplied by a user defined input (*ifact*), which is in general equal to unity. To create the coarse grid, the baseline grid sources were used but with the source sizes increased by $\sqrt{2}$. This lead to approximately 90,000 faces on the surface of the aircraft and a total of 2.85×10^6 cells (mixed tetrahedrons and prisms). The viscous spacing and growth rate were left unchanged compared to the baseline mesh. For the fine grid, the source sizes on the aircraft surface was divided by $\sqrt{2}$ with the outer boundary spacing left unchanged. This resulted in approximately 220,000 faces on the aircraft surface and 10×10^6 cells (mixed tetrahedrons and prisms). The geometric cell growth rate in the wall-normal direction was reduced from 1.30 to 1.25. This relatively simple procedure provided a sufficient approach to examining grid sensitivity in the complex configuration considered in this work.

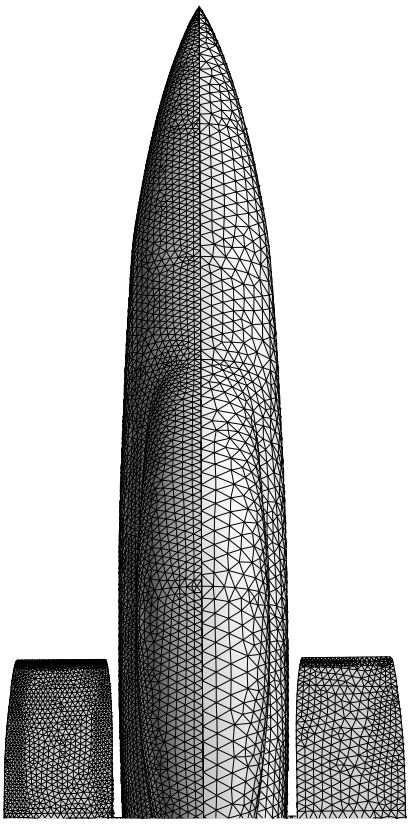

Fig. 4 Surface meshes on the nose for the coarse grid (2.85×10^6 cells) and fine grid (10.0×10^6).

Results

The computations were performed of the flow over a clean F-15E with no control deflections at $\alpha = 65°$ and zero sideslip. Boeing provided the authors with a stability and control database for the F-15E that was developed from a comprehensive spin testing program (courtesy of Ken Walck and Glen Peters of Boeing Military). Two stable spin conditions are detailed, including data for symmetric and asymmetric fuel loads. The aircraft with symmetric loading maintains a stable spin at 65° angle of attack. The performance of the computational model is first investigated at the same fixed angle of attack as for the stable spins prior to future attempts at prediction of the spin. All simulations were performed at the flight test conditions: a Mach number of 0.3 and standard day 30,000 feet.

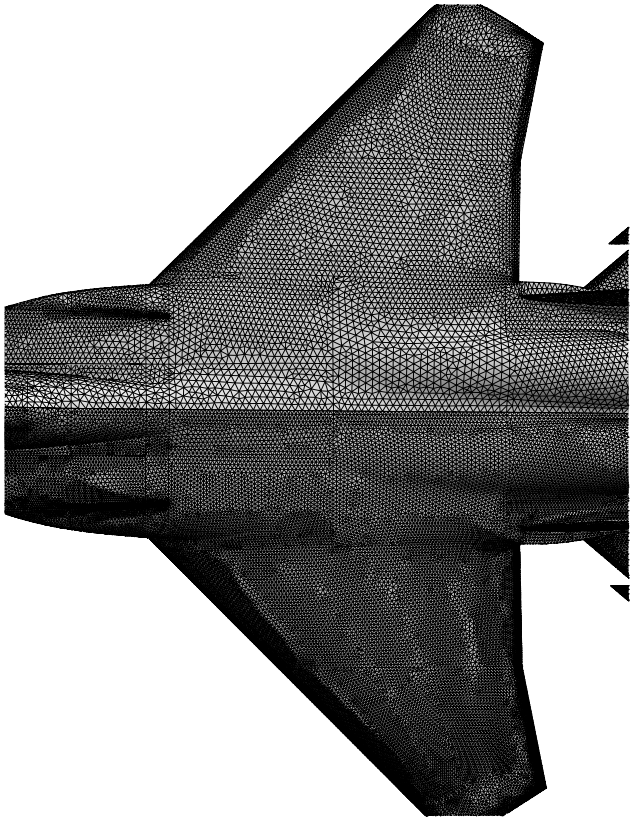

Fig. 5 Surface meshes on the wing for the coarse grid (2.85×10^6) and fine grid (10.0×10^6).

Fig. 6 Surface meshes on the tail for the coarse grid (2.85×10^6) and fine grid (10.0×10^6).

This resulted in a chord-based Reynolds number of 13.6×10^6.

Unsteady RANS (URANS) calculations did not not exhibit any significant unsteadiness and were equivalent to steady RANS predictions. The RANS results presented in this manuscript are of the steady-state flow, computed using a local CFL of 10^6, to give the most efficient convergence to steady state. The Spalart-Allmaras model presented above was employed in the RANS solutions. All DES calculations were performed with a minimum non-dimensional timestep of 0.01 (made dimensionless using the mean chord and freestream velocity). Because of the tight clustering in the boundary layer at high Reynolds number, this lead to a maximum CFL of over 500,000. The CFL outside the boundary layer was on the order of unity, as recommended by Spalart.[14] Since the boundary layer is treated by RANS it is not expected to be a source of instabilities, and therefore large CFL numbers are not problematic if the flow solver can stably integrate the discretized system.

Side-by-side comparisons of DES and RANS predictions across the symmetry plane are shown in Figures 7 and 8. The contours and isosurfaces of vorticity are an example in a complex configuration of the feature-resolving capacity of DES in its "LES mode", resolving the unsteady, geometry-dependent flow features.

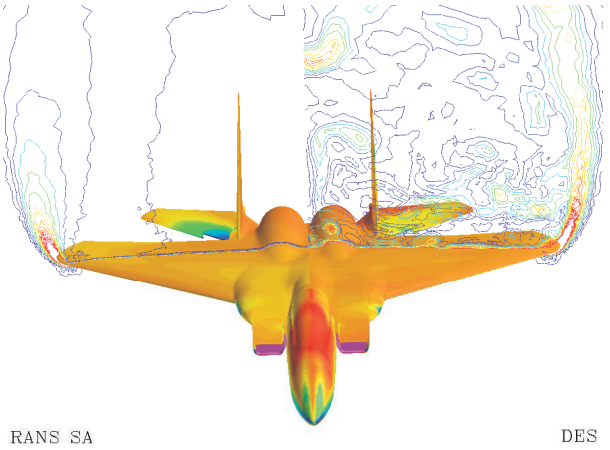

Fig. 7 Vorticity contours along a section of the F-15E from the baseline-grid calculations. Aircraft surface colored by pressure. DES predictions in right-half plane, S-A results in the left-half plane.

A timestep study was conducted using the baseline grid to assess the temporal accuracy of the DES predictions. For these runs, two Newton sub-iterations were used. The temporal evolution of the lift coefficient C_L for the two simulation techniques are compared to the Boeing database in Figure 9. Shown are lift histories from computations on the baseline grid (5.9×10^6 cells) and for three timesteps. A 5% error bar has been placed on the measurements since the expected accuracy of the Boeing database for this angle of attack is around 5% (Peters, private communication). The RANS calculation is converged within 3,000 iterations. The running time average for DES seems to have stabilized near the conclusion of the run, although it is not possible to rule out that still longer time integration may slightly influence the mean. Figure 9 shows that the averaged lift coefficient appears to be negligibly affected by changes in timestep. Frequency spectra of the normal force are plotted in Figure 10 for the three timesteps. Spectral densities of the normal force fluctuations are larger in the finest timestep run, with a portion of the spectra yielding a $-5/3$ slope. Note, however, that the spectra continue to improve as the timestep is reduced, showing that there remains an influence of the timestep on the higher frequencies of the solution.

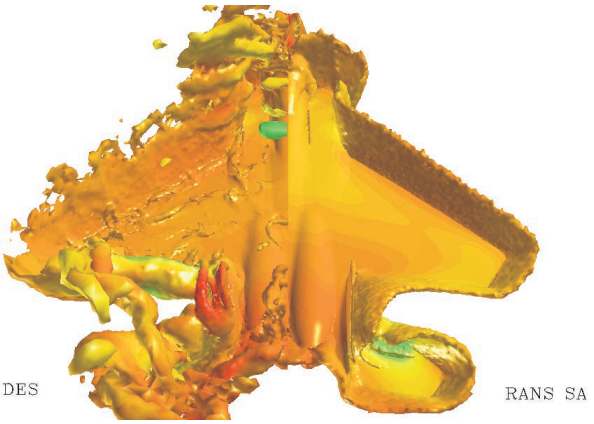

Fig. 8 Vorticity isosurface from baseline-grid calculations (colored by pressure). DES predictions in left-half plane, S-A results in the right-half plane.

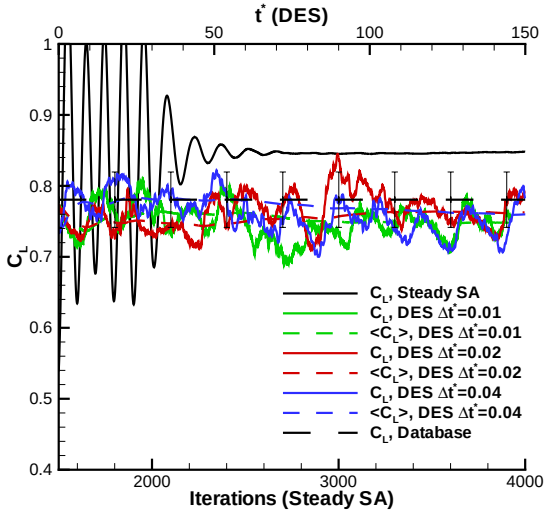

Fig. 9 Influence of timestep on lift coefficient history. Calculations performed on medium grid.

DES calculations were performed on the full aircraft

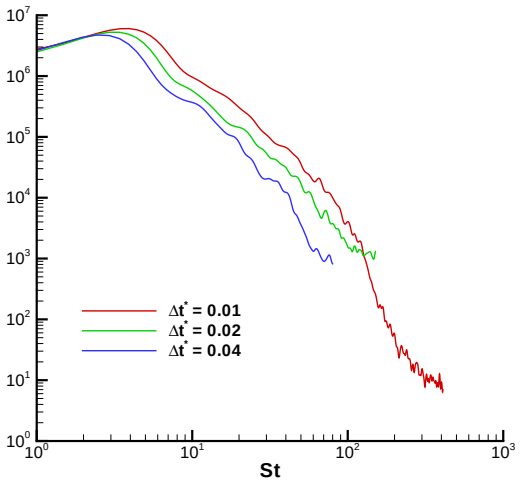

Fig. 10 Frequency spectra of the normal force. Curves in the figure from the baseline-grid computation.

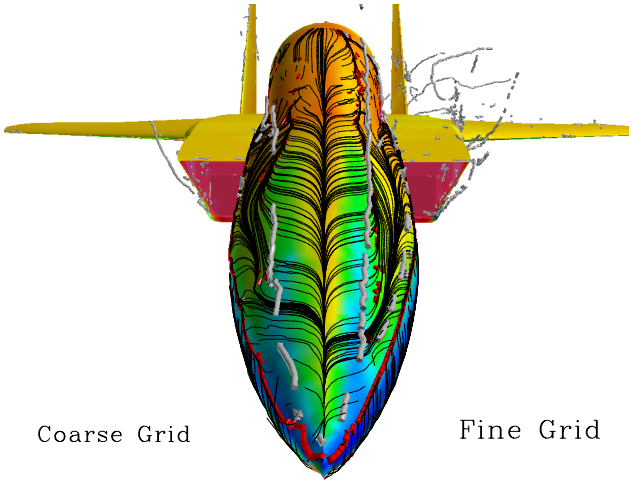

Fig. 11 Surface flows and separation line prediction along the forebody. Coarse-grid prediction in left-half plane, fine-grid prediction in right-half plane.

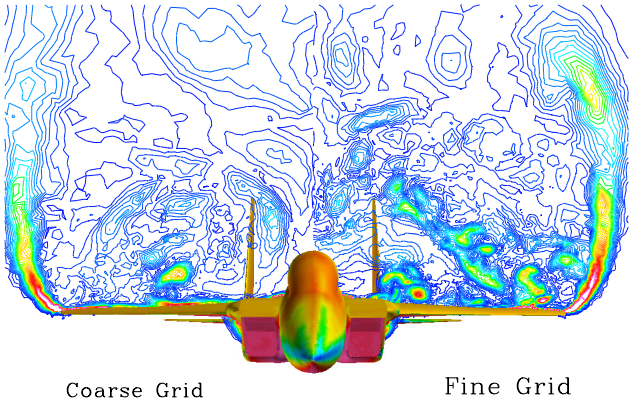

Fig. 12 Instantaneous vorticity contours at 680 inches behind the aircraft reference point. Coarse-grid prediction in left-half plane, fine-grid result in right-half plane.

by mirroring the baseline half-aircraft grid, to yield a mesh with 11.8×10^6 cells. The lift and drag coefficients matched the half-aircraft-grid results to within 2%. Unfortunately, processing the stored solutions is prohibitive given current computing capabilities, limiting detailed analysis of structural features.

For the subsequent computations used to investigate grid convergence, the non-dimensional timestep was fixed at 0.014 and the number of Newton sub-iterations increased to three.

Flow visualization comparisons are made between the coarse and fine grids on an instantaneous DES solution in Figures 11 and 12. Figure 11 uses the auto detection features of fieldview to show surface streamlines (black), vortex cores (grey) and separation lines (red) along the forebody for the two grids. The surface is colored by pressure. The coarse grid appears to be under-resolved with a slightly delayed formation of the secondary separation. The vortex is also less coherent as indicated by the separation and reattachment lines. One view of the resolution of unsteady flow features is accomplished by examination of the vorticity in a cutting plane shown in Figure 12. The LES character of DES will yield a wider range of scales as grid spacings are reduced, an effect clearly apparent in the figure. Note that even the coarse grid resolves at least some unsteady flow features – with a few small structures visible above the wing.

The time-averaged drag, lift, and moment coefficients along with their percentage errors compared to the Boeing database are summarized in Table 1 and Table 2. The S-A predictions are relatively accurate in the mean, an interesting finding given the model is applied to prediction of a flow far from its calibration range. Note that for the current configuration at high angle of attack the prediction of flow separa-

		C_L	C_D	C_M
	database	0.781	1.744	-0.466
DES	coarse	0.747	1.677	-0.431
	medium	0.736	1.616	-0.495
	fine	0.759	1.648	-0.457
S-A	coarse	0.855	1.879	-0.504
	medium	0.852	1.867	-0.523
	fine	0.860	1.880	-0.507

Table 1 Averaged lift, drag, and moment coefficients.

		$\%C_L$	$\%C_D$	$\%C_M$
DES	coarse	-4.25	-3.86	-7.62
	medium	-5.70	-7.35	6.10
	fine	-2.81	-5.52	-2.00
S-A	coarse	9.49	7.73	8.17
	medium	9.09	7.05	12.22
	fine	10.22	7.78	8.72

Table 2 Percentage errors in lift, drag, and pitching moment.

tion is somewhat less difficult than at lower α. This feature lessens modeling error and assists in obtaining more accurate predictions. The S-A results show little sensitivity to the grid refinement except for the pitching moment. The DES results show more variation with the grid, some of which may be an indicator of the need to time-average over a longer period. In general, Table 2 shows that the DES predictions are more accurate with respect to the flight-test data, with percentage errors smaller by as much as a factor of two in the drag coefficient predictions, for example. The largest discrepancy for both simulation techniques occurs in the moment coefficient, which is over-predicted (in a negative sense) by about 10% in the S-A runs. Viewed in light of the expected accuracy of the Boeing database for this angle of attack around 5%, the DES predictions are certainly satisfactory. Any further improvements would be within the estimated error and would not necessarily indicate a more accurate method.

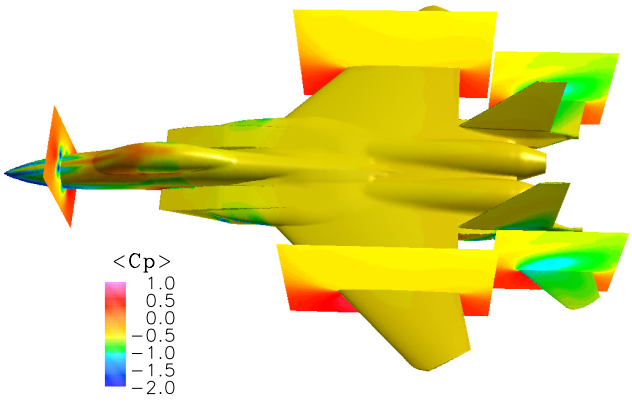

Fig. 13 Cutting planes for the pressure coefficient slices in Figures 14 through 17. Contours are time-average pressure coefficient on the fine grid for DES.

In an effort to understand the source of the differences between the RANS and DES predictions with grid refinement, the pressure coefficient from the (steady state) RANS is compared to the time average of the DES predictions. Slices are taken on the forebody, wing, and horizontal stabilizer as shown in Figure 13. Significant changes with both grid refinement and model are observed on the forebody in Figures 14 and 15. In the figures, $\theta = 0°$ is on the windward plane of symmetry, while $\theta = 180°$ is in the leeward plane of symmetry. As evidenced by the variation in C_p, RANS and DES show an increase in strength of both the primary and secondary vortices shed around the forebody from the coarse to the fine grid. The baseline grid, however, has a stronger primary vortex and a weaker secondary structure compared to the finest mesh. This reversal in vortex strengths as the grid is refined is not yet fully understood. One possible explanation is that small changes in grid orientation on the nose may result in slight differences in the structure of the vortex formation. Such an explanation would be consistent with previous work that has shown the flow near forebodies is sensitive to small disturbances near the apex[16] at these high angles of attack. The overall trend with grid refinement, however, is as expected – stronger vortices as the grid is refined and improved resolution of vortical motions.

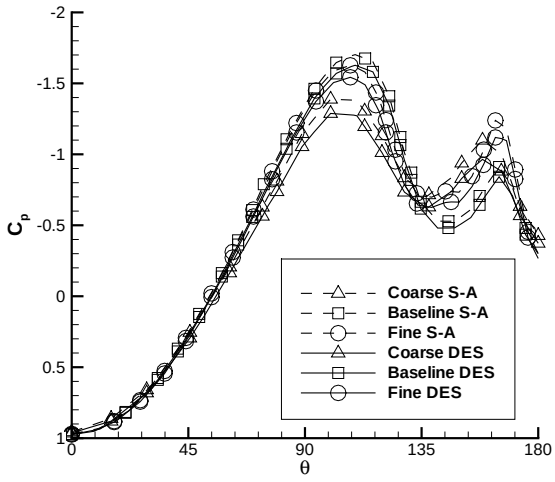

Fig. 14 Pressure coefficients on the F-15E forebody, 200 inches from the aircraft datum.

Figure 16 suggests that both DES and RANS are yielding a grid-converged solution for the flow over the wing. DES predicts a relatively flat profile in C_p that is the norm on a wing with separation, while the RANS predicts a more varied pressure distribution. Overall, however, the RANS prediction remains relatively close to the DES results, unlike solutions of canonical flows such as that around a two-dimensional NACA airfoil at high angle of attack.[8] The relatively strong coherent vortex shedding around two-dimensional shapes such as an airfoil or circular cylinder remains problematic for RANS because of the inability of these models to accurately account for, among other features, the modulation in vortex shedding. The flow over the F-15E appears not as strongly dominated by coherent shedding over a limited frequency band, lessening the need

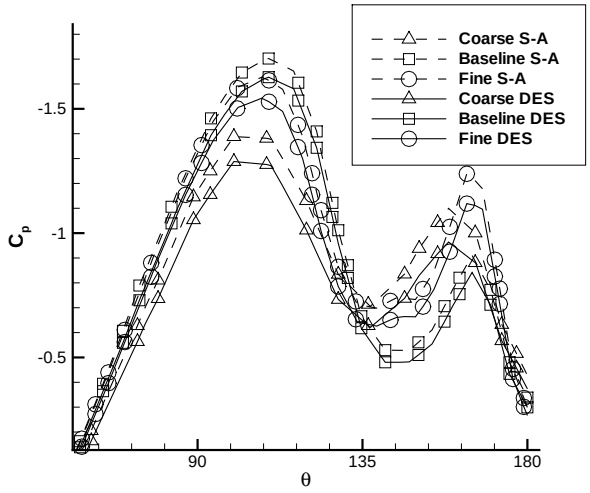

Fig. 15 Pressure coefficients on the F-15E forebody, 200 inches from the aircraft datum – close-up.

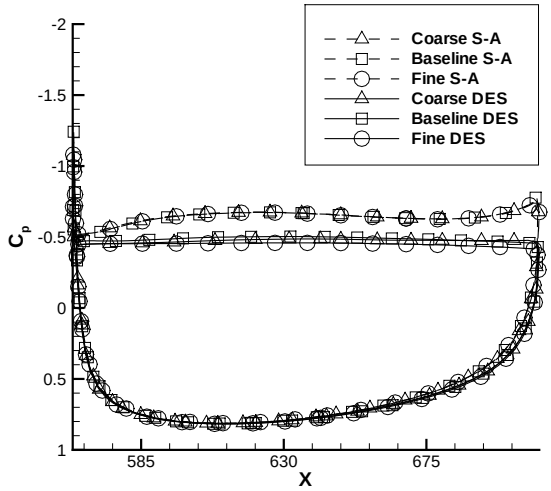

Fig. 16 Pressure coefficients on the F-15E wing, 158 inches from the aircraft centerline.

for RANS models to account for features such as force modulation.

The pressure coefficient on the horizontal stabilizer shows more significant changes with variations in model and grid resolution as shown in Figure 17. The differences between the baseline and fine grids for RANS are virtually identical suggesting a grid converged solution. The DES results for the baseline grid differ significantly from both the coarse and fine grids. DES time-averaged contours of pressure coefficient over the entire horizontal stabilizer are plotted for the three grids in Figure 18. Although Figure 17 makes it appear that the coarse and fine grids are giving similar solutions, Figure 18 shows that the surface pressures around the sawtooth are quite different. A

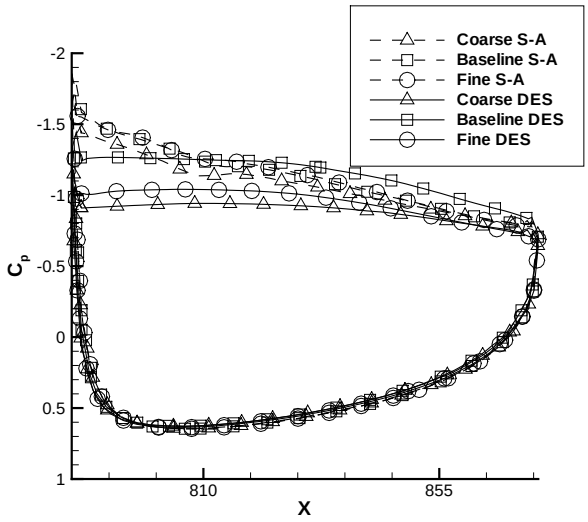

Fig. 17 Pressure coefficients on the F-15E horizontal stabilizer, 120 inches from the aircraft centerline.

potential explanation could be in the nature of DES. As a coarse grid is refined, the eddy viscosity may become too low for a RANS calculation, but the grid may be insufficient for an LES calculation. Thus the solution may deteriorate prior to improving. In the abscense of any experimental data, or a grid converged solution on the horizontal stabilizer, it is difficult to determine the cause of the reversal. Figure 19 presents instantaneous contours of vorticity for the baseline and fine grids. The fine grid seems to be much improved over the baseline grid in its capability to provide LES resolution.

Overall it appears that, while the predictions are not completely grid converged in either RANS or DES when examined in detail in particular regions of the domain, the overall forces are only weakly sensitive to grid refinement over the range examined. The lift and drag show small variations for each technique, likely due to the fact that the wing is well resolved. The larger variations in pitching moment are due to the variations in pressure on the nose and horizontal stabilizer, which have a strong effect on the moment due to the long moment arm for these parts of the geometry.

Summary

For the F-15E, the present DES calculations are probably one of the first applications of a turbulence-resolving technique to full aircraft at flight Reynolds numbers in which turbulent boundary layers on the vehicle were represented without recourse to wall functions (i.e., with grid spacings within one viscous unit at the wall). Both DES and RANS were subjected to a range of grid refinement of approximately a factor of two in each coordinate direction near the surface of the aircraft. The RANS results showed strong evidence of

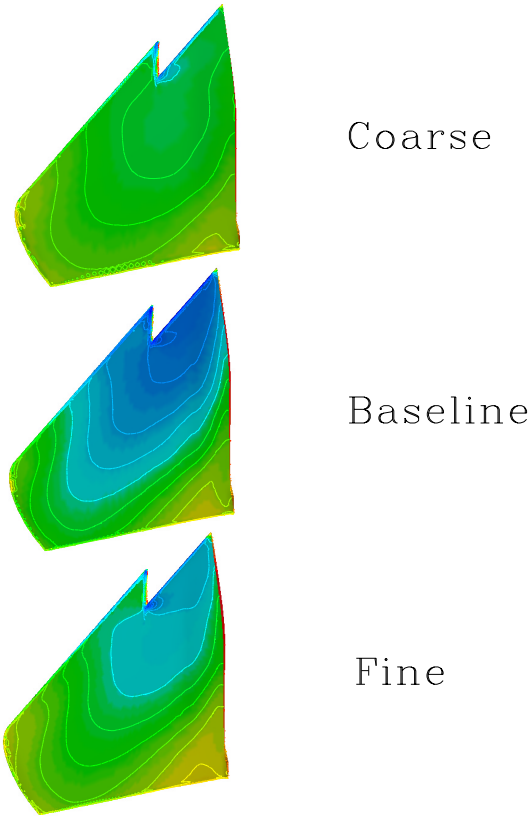

Fig. 18 DES time averaged contours of pressure on the horizontal stabilizer for the three grids.

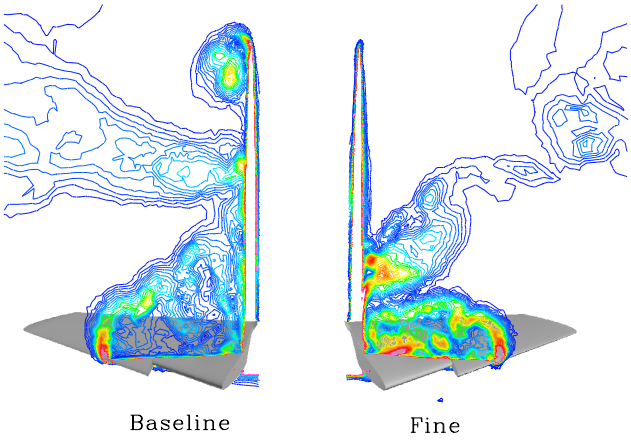

Fig. 19 Instantaneous vorticity contours in the tail region. the .

grid convergence in the overall forces. DES predictions showed slightly more sensitivity to grid refinement, although pressures on the wing are essentially grid converged. Pressure distributions on the forebody, wing, and horizontal stabilizer suggest that the horizontal stabilizer and forebody are slightly underesolved. One outcome of these observations is motivation for the use of adaptive gridding. Computation of the full aircraft had little effect on the integrated forces compared to the half-aircraft simulations. A timestep study was performed in the DES showing a reasonable resolution of the LES content of the solution, though complete convergence with respect to the timestep was not achieved.

The predicted lift, drag, and pitching moments from both RANS and DES were accurate in terms of their agreement with the Boeing database, with DES yielding slightly superior predictions. The adequate performance in the RANS was somewhat surprising given the accuracy problems faced by RANS in massively separated flows in canonical geometries such as a two-dimensional NACA airfoil at similar angle of attack.[8] Other configurations such as the two-dimensional solution around circular cylinders is also difficult to predict using RANS.[15] In other massively separated flows, however, such as that around a sphere, RANS predictions are adequate.[17] The three-dimensional character of the flow over the F-15E may assist RANS in providing a reasonable description of the mean. That aspect, combined with the fact that separation prediction is less a challenge than at lower angles of attack, help to lessen modeling errors, perhaps contributing to the adequate performance reported in this manuscript. However, while global quantities such as lift, drag, and moment were reasonable, RANS predictions failed to produce any significant unsteadiness in the computed solutions, while DES resolved a wider range of length and time scales as the grid density was increased. This would seem to be a positive development in extensions of DES to areas such as aero-elasticity and aero-acoustics.

Acknowledgements

The authors gratefully acknowledge the support of AFOSR Grant F49620-00-1-0050 (Program Manager: Dr. Tom Beutner). The authors are also grateful for the assistance of Glen Peters, Dr. Ken Walck, and Dr. Walt Labozzetta of Boeing Military, who provided the stability and control database and the F-15E geometry. Dr. Misha Strelets provided results and grids from his group's NACA 0012 calculations to help assess Cobalt accuracy in DES. Mr. Matthieu Chapelet and Cadet Kory Klismith have assisted with grid generation and post-processing. Cadet Warren Carroll and Cadet Alan VantLand aided in post-processing the F-15E results. Thanks to Fieldview for allowing the authors to beta test the new capability to do surface flows, which was used for Figure 11. Finally, the project would not have been possible without the support and cpu hours at NAVO MSRC and Maui HPCC.

References

[1]Peters, G. and Walck, K., "Excerpts from the F-15E Stability and Control Database", *Personal Communication*, Dec. 2000.

[2]Spalart, P.R., Jou, W.H., Strelets, M. and Allmaras, S.R., 1997, "Comments on the Feasibility of LES for Wings, and on a Hybrid RANS/LES Approach,", *First AFOSR International Conference on DNS/LES*, Ruston, Louisiana, USA.

[3]Strang, W.Z., Tomaro, R.F, Grismer, M.J., 1999, "The Defining Methods of Cobalt$_{60}$: a Parallel, Implicit, Unstructured Euler/Navier-Stokes Flow Solver," *AIAA 99-0786,* January 1999.

[4]Grismer, M. J., Strang, W. Z., Tomaro, R. F. and Witzemman, F. C., "Cobalt: A Parallel, Implicit, Unstructured Euler/Navier-Stokes Solver," *Advances in Engineering Software*, Vol. 29, No. 3-6, pp. 365—373, 1998.

[5]Tomaro, R.F., Strang, W.Z., and Sankar, L.N., 1997, "An Implicit Algorithm for Solving Time Dependent Flows on Unstructured Grids," *AIAA 97-0333*, January 1997.

[6]Spalart, P.R. and Allmaras, S.R., 1994, "A One-Equation Turbulence Model for Aerodynamic Flows," *La Recherche Aerospatiale* **1**, pp. 5-21.

[7]Spalart, P.R. (2000), "Strategies for Turbulence Modeling and Simulations", *International Journal of Heat and Fluid Flow*, **21**, p. 252-263.

[8]Shur, M., Spalart, P. R., Strelets, M., and Travin, A, 1999, "Detached-Eddy Simulation of an Airfoil at High Angle of Attack", 4th Int. Symp. Eng. Turb. Modelling and Measurements, Corsica, May 24-26, 1999.

[9]Gottlieb, J.J. and Groth, C.P.T., 1988, "Assessment of Riemann Solvers for Unsteady One-Dimensional Inviscid Flows of Perfect Gases", *Journal of Computational Physics*, **78**, pp. 437-458.

[10]Karypis, G., Schloegel, K. and Kumar, V., 1997, "ParMETIS: Parallel Graph Partitioning and Sparse Matrix Ordering Library Version 1.0", University of Minnesota, Department of Computer Science, Minneapolis, MN 55455, July 1997.

[11]Squires, K.D., Forsythe, J.R. Spalart, P.R., 2001, "Detached-Eddy Simulation of the separated flow around a forebody cross-section", *Direct and Large-Eddy Simulation IV*, ERCOFTAC Series – Volume 8, B.J. Geurts, R. Friedrich and O. Metais, editors, Kluwer Academic Press, pp. 481-500.

[12]Forsythe, J.R., Hoffmann, K.A., Dieteker, F.-F., "Detached-Eddy Simulation of a Supersonic Axisymmetric Base Flow with an Unstructured Flow Solver," *AIAA 00-2410*, June 2000.

[13]Pirzadeh, S., 1996, "Three-dimensional Unstructured Viscous Grids by the Advancing Layers Method," *AIAA Journal*, **34**, pp. 43-49.

[14]Spalart, P., "Young-Person's Guide to Detached-Eddy Simulation Grids," *NASA CR 2001-211032.*

[15]Travin, A., Shur, M., Strelets, M. and Spalart, P.R. (2000), "Detached-eddy simulations past a circular cylinder", *Flow, Turbulence, and Combustion*, **63**, pp. 293-313.

[16]Wurtzler, K.E., "An Effectivness Study of F-15 Forebody Flow Analysis Using Cobalt," *AIAA Paper 99-0536*, January 1999.

[17]Constantinescu, G.S. and Squires, K.D., 2000, "LES and DES investigations of turbulent flow over a sphere", *AIAA Paper 2000-0540.*